III. 平成２３年度　業績一覧

研究成果の刊行に関する一覧表

雑誌

発表者氏名	論文タイトル名	発表誌名	巻号	ページ	出版年
駒野　淳					
Takizawa M, Miyauchi K, Urano E, Kusagawa S, Kitamura K, Naganawa S, Murakami T, Honda M, Yamamoto N, Komano J*.	Regulation of the susceptibility of HIV-1 to a neutralizing antibody KD-247 by non-epitope mutations distant from its epitope.	AIDS.			In press.
Nomura W, Hashimoto C, Ohya A, Miyauchi K, Urano E, Tanaka T, Narumi T, Nakahara T, Komano J, Yamamoto N, Tamamura H.	Synthetic C34 Trimer of HIV-1 gp41 Shows Significant Increase of Inhibition Potency.	Chem Med Chem.			In press.
Watanabe T, Urano E, Miyauchi K, Ichikawa R, Hamatake M, Misawa N, Sato K, Ebina H, Koyanagi Y, Komano J*.	The hematopoietic cell-specific Rho GTPase inhibitor ARHGDIB/D4GDI limits HIV-1 replication.	AIDS Res Hum Retroviruses.			In press.
Imadome K, Yajima M, Arai A, Nakagawa-Nakagawa A, Kawano F, Ichikawa S, Shimizu N, Yamamoto N, Morio T, Ohga S, Nakamura H, Ito M, Miura O, Komano J, Fujiwara S*.	CD4-positive T cells have a critical role in the proliferation of EBV-infected T and NK cells.	PLOS Pathog.			In press
Urano E, Kuramochi N, Tomoda H, Takebe Y, Miyauchi K, Komano J*, Morikawa Y*.	A Novel Postentry Inhibitor of Human Immunodeficiency Virus Type 1 Replication Screened by Yeast Membrane-associated Two-hybrid System.	Antimicrob Agents Chemother.	Sep;55(9)	4251-60	2011
Aoki T, Miyauchi K, Urano E, Ichikawa R, Komano J.	Protein transduction by pseudotyped lentivirus-like nanoparticles.	Gene Ther.	Sep;18(9)	936-41	2011

Miyauchi K, Urano E, Yoshiyama H, Komano J*.	Cytokine signatures of transformed B cells with distinct EBV latencies as a potential diagnostic tool for B cell lymphoma.	Cancer Sci.	Jun;102(6)	1236-41	2011
Yanagita H, Urano E, Matsumoto K, Ichikawa R, Takaesu Y, Ogata M, Murakami T, Wu H, Chiba J, Komano J, Hoshino T.	Structural and biochemical study on the inhibitory activity of derivatives of 5-nitro-furan-2-carboxylic acid for RNase H function of HIV-1 reverse transcriptase.	Bioorganic & Medicinal Chemistry.	19	816-25	2011
駒野　淳.	止まらないエイズウイルス流行の拡大.	中央論評			In press.
星野　忠次					
W. Li, J. Shen, Y. Tang, T. Hoshino	Exploring coumarin egress channels in human cytochrome P450 2A6 by random acceleration and steered molecular dynamics simulations	Proteins	79(1)	271-281	2011
MD Iqbal Mahmood, Yuri Matsuo, Saburo Neya, Tyuji Hoshino	Computational Analysis on the Binding of Epitope Peptide to Human Leukocyte Antigen Class I Molecule A*2402 Subtype	Chem. Pharm. Bull.	59(10)	1254-1262	2011
Hitomi Yuki, Teruki Honma, Masayuki Hata, Tyuji Hoshino	Prediction of sites of metabolism in a substrate molecule, instanced by carbamazepine oxidation by CYP3A4	Bioorg. Med. Chem.	20(2)	775-783	2012

Ⅳ. 平成２３年度　刊行物別刷（抜粋）

Gene Therapy (2011) 18, 936–941

www.nature.com/gt

SHORT COMMUNICATION

Protein transduction by pseudotyped lentivirus-like nanoparticles

T Aoki[1,2], K Miyauchi[1,2], E Urano[1], R Ichikawa[1] and J Komano[1]

A simple, efficient and reproducible method to transduce proteins into mammalian cells has not been established. Here we describe a novel protein transduction method based on a lentiviral vector. We have developed a method to package several thousand foreign protein molecules into a lentivirus-like nanoparticle (LENA) and deliver them into mammalian cells. In this proof-of-concept study, we used β-lactamase (BlaM) as a reporter molecule. The amino-terminus of BlaM was fused to the myristoylation signal of *lyn*, which was placed upstream of the amino-terminus of *Gag* (BlaM-gag-pol). By co-transfection of plasmids encoding BlaM-gag-pol and vesicular stomatitis virus-G (VSV-G) into 293T cells, LENA were produced containing BlaM enzyme molecules as many as Gag per capsid, which has been reported to be ~5000 molecules, but lacking the viral genome. Infection of 293T and MT-4 cells by VSV-G-pseudotyped BlaM-containing LENA led to successful transduction of BlaM molecules into the cell cytoplasm, as detected by cleavage of the fluorescent BlaM substrate CCF2-AM. LENA-mediated transient protein transduction does not damage cellular DNA, and the preparation of highly purified protein is not necessary. This technology is potentially useful in various basic and clinical applications.
Gene Therapy (2011) **18,** 936–941; doi:10.1038/gt.2011.38; published online 31 March 2011

Keywords: LENA; BlaM; Gag; protein transduction; lentiviral vector

INTRODUCTION

When viruses infect cells the viral contents are released. A virus can, therefore, be considered as a protein transduction vehicle into a target cell if a large number of foreign proteins are packaged per virion. A lentiviral vector, approved for human gene therapy,[1] has been produced by transfecting 293T cells with four plasmids: the gene transfer vector that provides the viral genome packaged into the virion, and three plasmid vectors, each expressing *gag–pol*, *rev* or the vesicular stomatitis virus-G (VSV-G) genome.[2–4] The *gag–pol* expression vector produces Gag and Gag-pol in a ratio of ~20:1 because of the frameshift signal positioned between the *gag* and *pol* open reading frames.[5] Gag ($Pr55^{Gag}$) is a viral structural protein that traffics to the plasma membrane aided by its amino-terminal myristoyl group, and self-oligomerizes at the plasma membrane to form a spherical structure.[6] The expression of Gag alone leads to the production of an enveloped virus-like particle (VLP) of ~100 nm in diameter, consisting of ~5000 Gag molecules.[7]

When the *gag–pol* expression vector is used to produce VLP, both Gag and Gag-pol proteins, a total of 5000 molecules,[7] form the lentiviral nanoparticles in which approximately one-twentieth of the VLP-forming protein is Gag-pol.[5] The VLP produced by the *gag–pol* expression vector undergoes maturation whereby Gag is processed by the protease made from Pol. Gag is cleaved into $p17^{MA}$, $p24^{CA}$ and other smaller fragments. This changes the shape of the VLP core from doughnut shape to bullet shape, as visualized by electron microscopy. Mediated by VSV-G, the mature VLP envelope fuses to the cell membrane more efficiently than the immature VLP.[8] In accordance with this process, if a foreign protein is fused to lentiviral Gag, a large number of foreign proteins should be transduced into mammalian cells. In this work, the lentiviral vector has been engineered to achieve this goal.

By co-transfecting two plasmid vectors, each expressing *gag–pol* or VSV-G, the lentivirus-like nanoparticles (LENA) can be produced with a VSV-G envelope (Figure 1a). These particles undergo maturation, and should be highly competent for promoting fusion of LENA envelope to the cell membrane. The VSV-G-pseudotyped LENA should be capable of releasing viral content into the target cells. We have named this process 'pseudoinfection' because it mimics viral infection, but is not accompanied by integration of the viral genome into chromosomal DNA.

We have previously shown that substitution of the human immunodeficiency virus type 1 (HIV-1) Gag myristoylation signal with the phospholipase C-δ 1 pleckstrin homology (PH) domain, or attachment of heterologous myristoylation signals to the amino-terminus of Gag, increases the production of lentiviral vector.[9,10] In these studies we used the human codon-optimized *gag–pol* to maximize viral protein synthesis. The infectivity of these pseudovirions was comparable with that of the wild-type (WT) counterpart. This is noteworthy because modification of Gag often results in reduction of viral productivity and infectivity.[11,12] It has been reported recently that a protein transduction using murine leukemia virus is achievable by embedding a foreign gene in *gag*. However, the viral productivity and infectivity need to be improved by WT Gag-pol provided in *trans* upon viral production. These data suggest that by fusing a foreign protein to the amino-terminus of Gag and providing a membrane-targeting signal, it is possible to produce a high-titer, uniform, foreign protein-containing LENA without the need to co-transfect the WT Gag-pol expression plasmid. We tested whether the VSV-G-pseudotyped

[1]AIDS Research Center, National Institute of Infectious Diseases, Shinjuku-ku, Tokyo, Japan
Correspondence: Dr J Komano, AIDS Research Center, National Institute of Infectious Diseases, Toyama, 1-23-1, Shinjuku-ku, Tokyo 162-8640, Japan.
E-mail: ajkomano@nih.go.jp
[2]These authors contributed equally to this work.
Received 29 August 2010; revised 2 December 2010; accepted 3 January 2011; published online 31 March 2011

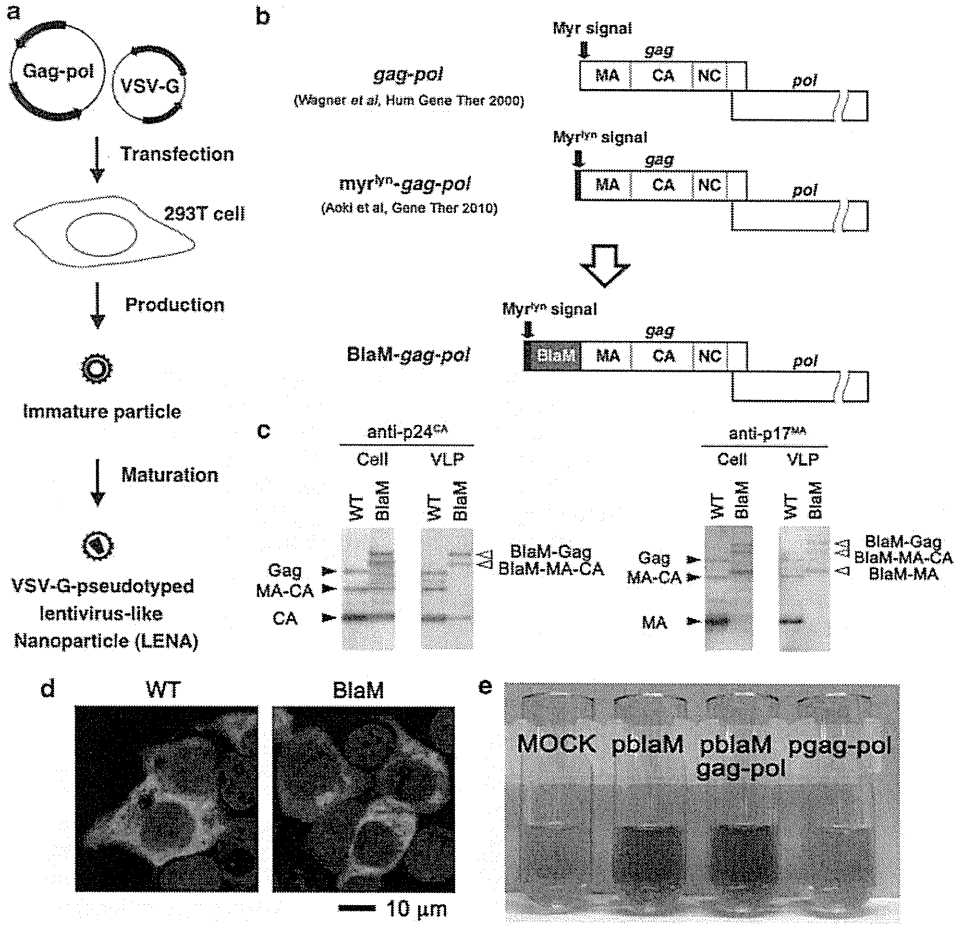

Figure 1 Production of a BlaM-containing LENA pseudotyped with VSV-G. (**a**) Schematic representation of production of VSV-G-pseudotyped LENA. Two plasmids are transfected into 293T cells, and LENA is recovered from the culture supernatant at 48 h post-transfection. The viral protease is activated after the VLP is released from the cell, and it mediates the maturation of the particles. (**b**) The structure of WT *gag–pol*, a mutant bearing the myristoylation signal of *lyn* (myr^{lyn}-*gag-pol*), and *blaM-gag-pol*. Gag is cleaved into p17^{MA} (MA), p24^{CA} (CA), nucleocapsid (NC) and other domains by the viral protease encoded in *pol*. In the myr^{lyn}-*gag-pol* and *blaM-gag-pol* constructs, the Gag translational initiation site and the myristoylation target residues were mutated to leucine and alanine to minimize internal translational initiation and myristoylation. (**c**) Verification of protein expression and VLP production of BlaM-gag-pol construct in 293T cells by western blot analysis using anti-p24^{CA} and anti-p17^{MA} antibodies. Shown are the analyses of cell lysates (Cell) transfected with p*gag-pol* (WT) or p*blaM-gag-pol* (BlaM), and the viral particles (VLP) collected from the culture supernatant of transfected cells. Pr55^{Gag} (~55 kDa, Gag), the Gag proteolytic cleavage intermediate MA–CA (~40 kDa) and the complete proteolytic cleavage product p24^{CA} (~24 kDa, CA) and p17^{MA} (~17 kDa, MA) are indicated by arrowheads. BlaM-Gag, BlaM-MA-CA and BlaM-MA have higher molecular weights because of the attachment of BlaM (~30 kDa) to the MA domain. (**d**) Immunofluorescence assay showing the distribution of WT Gag (WT) or BlaM-Gag (BlaM) in 293T cells transfected with p*gag-pol* or p*blaM-gag-pol*. Green and blue represent the anti-p24^{CA} monoclonal antibody-stained signal and the Hoechst 33258-stained nucleus, respectively. Magnification ×400; scale bar, 10 μm. (**e**) BlaM enzyme activity was tested by nitrocefin. Lysates from 293T cells transfected with p*blaM*, p*blaM-gag-pol*, *or* p*gag-pol* or untransfected cells (MOCK) were incubated with nitrocefin for 30 min at 37 °C.

LENA could serve as a protein transduction vehicle for mammalian cells using β-lactamase (BlaM) as a reporter.

RESULTS AND DISCUSSION

BlaM was chosen as reporter molecule because mammalian cells do not have BlaM activity. Also, a cell-membrane-permeable BlaM substrate is available, which can distinguish LENA content release from cellular endocytosis of LENA that can occur without membrane fusion.[13] *BlaM* was fused to the amino-terminus of *gag–pol*, and the *lyn* myristoylation signal was attached to the amino-terminus of *BlaM* (*BlaM-gag-pol*; Figure 1b). The codon usage of *gag–pol* has been human codon optimized, but bearing the natural −1 frameshift signal at the *gag–pol* junction.[14] Thus, the vector provides the natural Gag to Gag-pol ratio. The BlaM-gag-pol protein was produced in 293T cells as expected (Figure 1c). The *BlaM* construct produced VLP from the transfected cells, although the efficiency was less than with WT *gag–pol* (Figure 1c). The processing efficacy of Gag in BlaM VLP was less efficient compared with the WT as highlighted by the absence of free matrix domain (MA) signal in BlaM VLP, which was because of the lack of HIV-1 protease recognition motif between BlaM and MA (right panel, Figure 1c). In 293T cells transiently transfected with this plasmid, the BlaM-gag-pol fusion protein distribution was similar to that of the WT, although with some aggregation in the cytoplasm (Figure 1d). The BlaM-gag-pol fusion protein retained enzyme activity as demonstrated by its reaction with the BlaM substrate nitrocefin, which changed from a straw color to brown when incubated with

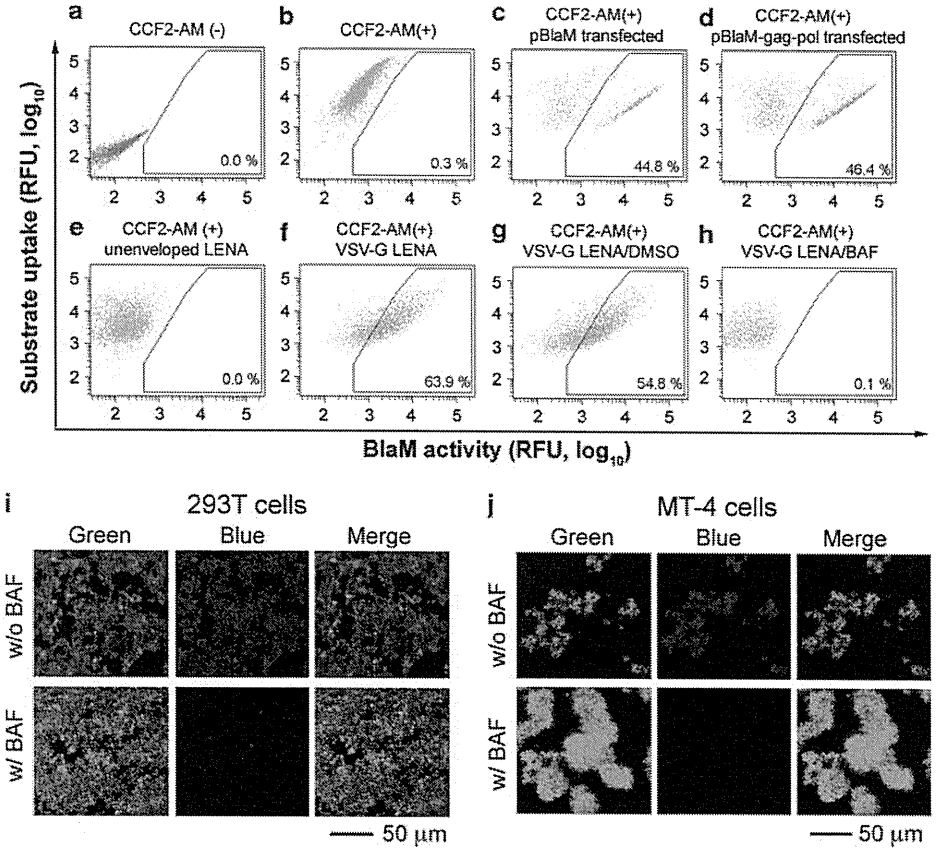

Figure 2 Flow cytometric analysis to measure the BlaM transduction into 293T cells by VSV-G-pseudotyped BlaM-LENA. The 293T cells were grown in 24-well plates and either transfected or pseudoinfected with LENA preparations. (**a**) Unstained 293T cells. (**b**) 293T cells loaded with CCF2-AM. (**c**, **d**) 293T cells were transfected with pBlaM (**c**) or pBlaM-gag-pol (**d**), and loaded with CCF2-AM at 48 h post-transfection before the flow cytometric analysis. (**e–h**) 293T cells were exposed to unenveloped BlaM-LENA (**e**) or VSV-G-pseudotyped BlaM-LENA (**f–h**). Cells were loaded with CCF2-AM at 2 h post-LENA exposure. (**g**, **h**) The VSV-G-dependent BlaM transduction was verified by exposing 293T cells with VSV-G-pseudotyped BlaM-LENA in the presence of bafilomycin A1 (BAF) at a concentration of 10 μg ml^{-1} (**h**). Dimethylsulfoxide (DMSO) was used as a control (**g**). The percentage of the gated population is noted in each panel. The *x* axis represents the blue fluorescence, reflecting the BlaM activity (relative fluorescent unit (RFU)). The *y* axis represents the green fluorescence, reflecting the substrate loading onto the cells. (**i**, **j**) Microscopic detection of BlaM transduction in 293T cells (**i**) or MT-4 cells (**j**) by VSV-G-pseudotyped BlaM-LENA. Cells were exposed to BlaM-LENA for 3 h, and loaded with CCF2-AM overnight at room temperature in the presence (10 μg ml^{-1}) or absence of BAF (w/BAF or w/o BAF, respectively). The bar represents 50 μm, magnification ×200.

lysates from 293T cells transfected with the BlaM-gag-pol expression vector (Figure 1e). The BlaM enzyme activity of BlaM-gag-pol was indistinguishable from that of WT BlaM (Figure 1e). BlaM enzyme activity was not detected in MOCK or p*gag-pol*-transfected cell lysates (Figure 1e).

Protein transduction into 293T cells was conducted by exposing target cells to VSV-G-pseudotyped BlaM-LENA, which mimics viral infection. The success of BlaM transduction into the target cell cytoplasm was judged by using the cytoplasm-retained BlaM substrate, CCF2-AM, which yields blue fluorescence upon cleavage by BlaM enzyme activity.

The 293T cells emitted green fluorescence when they were loaded with CCF2-AM (Figure 2, compare a vs b). When 293T cells were transfected with expression vectors for BlaM or the BlaM-gag-pol, substrate cleavage, as demonstrated by a shift to blue fluorescence, was detected in a discrete population of cells, representing a transfection efficiency of ~45% (Figures 2c and d). These data suggest that transduced BlaM-gag-pol has BlaM activity, consistent with the results of the nitrocefin assay (Figure 1e). When BlaM was transduced into 293T cells by VSV-G-pseudotyped BlaM-LENA, a significant shift from green to blue fluorescence was detected (63.9%, Figure 2f). The rightward shift of the signal along the *x* axis suggests that almost all the cells were transduced with BlaM by BlaM-LENA. BlaM transduction was dependent on VSV-G function as CCF2-AM cleavage was not detected by LENA lacking VSV-G (Figure 2e), and BlaM transduction was inhibited by bafilomycin A1 that blocks VSV-G-mediated membrane fusion (Figure 2, compare g vs h). The catalytic activity was visualized under the fluorescent microscopy. In agreement with the flow cytometric analysis, almost all the substrate-loaded 293T cells exposed to BlaM-LENA became blue fluorescent in experimental conditions comparable with the above experiments, and the catalytic activity was not detected when cells were treated with bafilomycin A1 (Figure 2i). The blue fluorescence was detected homogenously in the cell cytoplasm (Figure 2i). These data were reproduced in human T-cell line MT-4 (Figure 2j). Considering the critical dependence to VSV-G, it is highly unlikely that the BlaM activity was derived from the residual DNA/lipid mixture in the LENA preparation. The BlaM-transducing unit into 293T cells was $\sim 0.8 \pm 0.01 \times 10^9$ ml^{-1} as

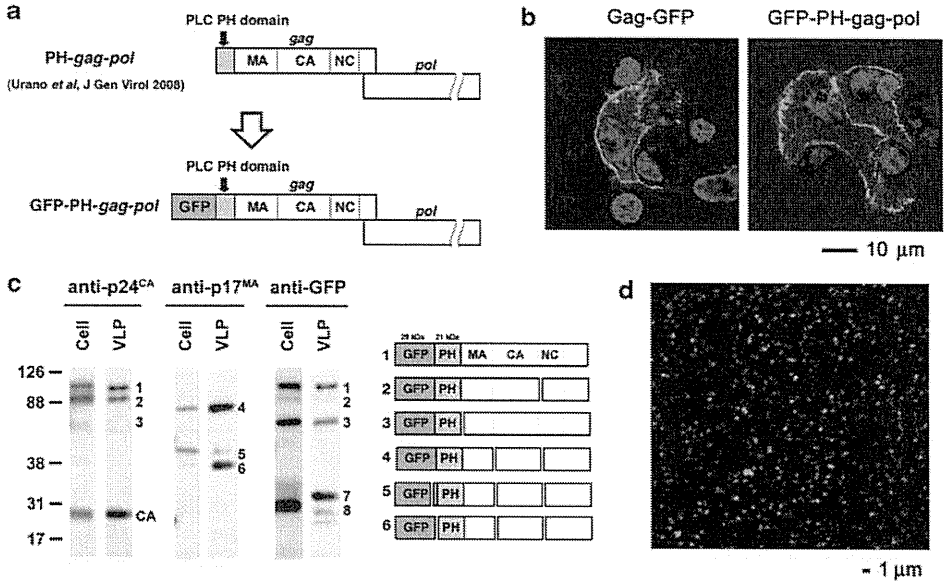

Figure 3 Production of a GFP-containing lentivirus-like nanoparticle for physical counting. (**a**) The structure of PH-*gag-pol* and GFP-PH-*gag-pol*. (**b**) The distribution of Gag-GFP and GFP-PH-gag-pol in transiently transfected 293T cells examined by confocal microscopy. The images were taken at 24 h post-transfection. The bar represents 10 μm, magnification ×630. (**c**) Verification of protein expression and VLP production of GFP-PH-gag-pol construct in 293T cells by western blot analysis using anti-$p24^{CA}$, anti-$p17^{MA}$ and anti-GFP antibodies. Shown are the analyses of cell lysates (Cell) transfected with pGFP-PH-*gag-pol* and the viral particles (VLP) collected from the culture supernatant of transfected cells. The numbers represent the proteolytic products as illustrated in the right panel estimated from the western blot analysis. (**d**) Confocal image of the GFP-PH-LENA on the slide glass. The bar represents 1 μm, magnification ×630.

estimated by the BlaM-LENA serial dilution (data not shown). Thus, 293T cells were exposed to ~1000-fold excess of BlaM-LENA.

We constructed GFP-PH-LENA to visualize the LENA particles (Figure 3a). In this construct, the PH domain from phospholipase C-δ 1 functions as the membrane targeting motif.[9,10] The GFP-PH-gag-pol was distributed at cell periphery, similar to Gag-GFP (Figure 3b). The VLP production by GFP-PH-gag-pol was verified in western blot analysis (Figure 3c). According to the estimated molecular weight of protease-mediated cleavage products, we speculate the possible protease recognition sites within green fluorescent protein (GFP), GFP–PH junction and PH–MA junction, although we did not intentionally reconstitute the HIV-1 protease recognition sites in these positions (Figure 3c). The GFP-encapsidated LENA preparations were spotted onto the poly-L-lysine-coated slide glass, and the captured LENA was imaged by the confocal microscopy. By counting the green fluorescent dot signals per unit area, we estimated the number of GFP-PH-LENA particles as $1.4 \pm 0.2 \times 10^9\ ml^{-1}$ (Figure 3d), which was similar to the BlaM-transduction unit of VSV-G-pseudotyped BlaM-LENA.

To test whether the lentivirus vector used to produce BlaM-LENA retained any viral infectivity, a lentivirus vector was produced carrying the luciferase gene, using the four plasmid system[9,10] with the BlaM-gag-pol construct, and then viral infectivity was assessed. Gene transduction by this lentiviral vector was undetectable. These data indicate that transfer to target cells by BlaM-LENA of an expressed, endogenous retroviral element from 293T cells is unlikely to occur. These data show that a protein transduction system based on LENA would have an extra level of safety compared with the protein transduction system based on a retroviral vector system.[11]

Protein transduction in a broad sense, referring to the transport of protein across the cell membrane, is a useful technique in experimental molecular biology. It does not require *de novo* transcription and translation, and the transferred protein functions immediately after the transduction. Proteins, however, do not easily pass through the plasma membrane. Historically, microinjection, electroporation and cell-permeable peptide motifs were used to introduce proteins into cells.[15–17] These methods, however, demand a highly purified protein, technical skill or specialized, costly equipment. Also, variable results have been obtained using different proteins and target cells. The need of a highly purified protein applies to protein lipofection to yield the reproducible results. A convenient, fast, highly efficient and reproducible protein transduction method has so far remained undeveloped. Such a technique would greatly help the generation of safe, induced pluripotent stem cells. LENA production is as straightforward as co-transfecting two plasmids into 293T cells without *trans*-complementing the WT *gag–pol* expression vector, and furthermore the therapeutic protein is protected from plasma proteases by a lipid bilayer. The target cell tropism can be controlled by well-established viral pseudotype techniques. Using LENA, a substantial number of protein molecules can be packaged into the nanoparticles, and the transduction procedure is as easy as exposing mammalian cells with LENA. There is no need to prepare highly purified proteins for the LENA system. Also, target proteins are post-translationally modified in human cells, which should be better than the protein modification in non-human organisms. It should also be possible to increase the amount of protein that can be delivered into cells by concentrating the LENA preparation. Physical counting of GFP-encapsidated LENA shows that a high-titer LENA preparation was casually produced. In this study, we did not introduce protease recognition sites into myristoylation signal-BlaM or -BlaM-MA junctions. By doing so, we would have possibly liberated the foreign protein from the precursor. This could result in infectious LENA particles as the free MA is in part important for the viral infectivity.[9]

Currently, few approaches are available for the incorporation of a foreign protein into retro- or lenti-viral VLP. The protein of interest

can be fused to the C-terminus of Gag or inserted into the middle of the Gag protein (for example, between the MA and CA).[11,12] Foreign protein fusion to the C-terminus of Gag would destroy the frameshift signal required to produce Gag-pol. Thus, Pol would no longer be produced. To maintain efficient pseudoinfection, the *gag–pol* expression vector must be provided in *trans* when the VLP is produced. The latter approach often results in reduced VLP yield. Thus, again, to increase the VLP yield, the *gag–pol* expression vector has to be co-transfected with the plasmid encoding Gag fused to the foreign protein. Co-transfection of the *gag–pol* expression vector is likely to reduce the amount of foreign protein per VLP, and lower its uniformity. It is, therefore, desirable not to co-transfect with the WT *gag–pol* expression plasmid. Alternatively, Vpr can be used to incorporate foreign proteins into lentiviral particles.[18] Only a few dozen protein molecules, however, are packed per particle, rendering this approach of little use in protein transduction. In summary, fusion of a foreign protein to the N-terminus of Gag has the advantages of producing uniform, high-titer and membrane fusion-competent VLP without *trans*-complementation by WT Gag-pol.

The disadvantages of the LENA system are the susceptibility of foreign proteins to viral protease and the restriction in the molecular sizes of foreign proteins. We have succeeded in generating Gag-LacZ VLP, suggesting that the production of LENA carrying a foreign protein with a molecular weight of ~100 kDa is feasible. The yield, however, of LENA gradually decreases as the molecular weight of the foreign protein increases. We did not detect proteolytic cleavage of BlaM by viral protease in LENA particles; however, when we tested the transcriptional regulator of HTLV-1 (human T-cell leukemia virus type 1), Tax, it was degraded by viral protease. To overcome these potential disadvantages, it is worth considering the use of only the minimal functional domain of a foreign protein and the destruction of potential protease recognition sites in the foreign protein without losing its function.

Lentiviral vectors have been approved for human gene therapy.[1] LENA does not contain a viral genome, and is unlikely to support the transfer of endogenous retrovirus-like elements; thus, the cellular genome is not threatened by LENA-mediated protein transduction. Thus, a major safety concern associated with retroviral or lentiviral vectors is alleviated, making LENA applicable for *in vivo* studies. Retroviral vectors are often used for induced pluripotent stem cell genesis.[19] However, they can damage the cellular genome, and transduced gene expression is difficult to shut off, which can lead to malignant transformation of induced pluripotent stem cells. To overcome this problem, a transient and efficient protein transduction method is needed. We believe that LENA addresses these issues. Altogether, our system has many advantages over currently available protein transduction protocols, suggesting that it should be considered for basic and clinical applications.

MATERIALS AND METHODS

Plasmids

The following oligonucleotides were annealed, and cloned into the *AfeI–AgeI* sites of pEGFP-C2 (Clontech, Palo Alto, CA, USA) to generate the p*lyn*MyEGFP-C2: 5′-GCTACCGGACTCAGATCTCGAGCTCAAGCTTCGAATTGC CACCATGGGATGTATTAAATCAAAAAGGAAAGACGATCCA-3′ and 5′-CCG GTGGATCGTCTTTCCTTTTTGATTTAATACATCCCATGGTGGCAATTCGA AGCTTGAGCTCGAGATCTGAGTCCGGTAGC-3′. The *SnaBI–EcoRI* fragment from p*lyn*MyEGFP-C2 was cloned into the corresponding sites of pPH-*gag-pol*,[9] generating p*lyn*MyGFP-*gag-pol*. The β-lactamase gene from pUC19 was amplified by the following primers: 5′-ACCGGTCAATCCAGAAACGCTGGTG AAAG-3′ and 5′-CAATTGCCAATGCTTAATCAGTGAGGC-3′. The *AgeI–MfeI* fragment of the PCR fragment was cloned into the *AgeI–EcoRI* sites of p*lyn*MyGFP-*gag-pol*, generating the p*blaM-gag-pol*. The expression vector for VSV-G was described previously.[20] The original codon-optimized HIV-1 *gag–pol* expression vector was described previously.[14] The Gag-GFP expression vector was described previously.[10] The pGFP-PH-*gag-pol* was constructed by inserting the *NdeI–PshAI* fragment from pEGFP-PLCd1 PH[21] into the corresponding sites of pPH-*gag-pol*.[9] pcDNA3 was obtained from Invitrogen (Tokyo, Japan).

Cells and transfection

The 293T cells, obtained from Invitrogen as 293FT cells (Invitrogen), were maintained in RPMI-1640 medium (Sigma, St Louis, MA, USA) supplemented with 10% fetal bovine serum (Japan Bioserum, Tokyo, Japan), 50 U ml^{-1} penicillin and 50 μg ml^{-1} streptomycin (Invitrogen), at 37 °C in a humidified 5% CO_2 atmosphere. Cells were transfected with DNA using Lipofectamine 2000 according to the manufacturer's protocol (Invitrogen), or calcium phosphate precipitation. To produce VSV-G-pseudotyped BlaM-LENA, equal amounts of pVSV-G and p*blaM-gag-pol* were transfected into 293T cells. Unenveloped BlaM-LENA was produced using pcDNA3 in place of pVSV-G.

Immunological detection

The detection of viral gene products by western blot analysis was performed as described previously,[22] except that the anti-p24^{CA} monoclonal antibody clone 183-H12-5C and the anti-p17^{MA} rabbit antiserum (NIH AIDS Research and Reference Reagent Program) were used. The immunofluorescent analysis was performed as described previously,[22] except that cells were fixed at 24 h post-transfection, and the following reagents were used: anti-p24^{CA} monoclonal antibody (clone 183-H12-5C), anti-mouse antibody conjugated with biotin (Invitrogen) and streptavidin conjugated with Alexa488 (Invitrogen).

Microscopy

Cells and GFP-encapsidated LENA were imaged by confocal fluorescence microscopy (LSM510 Meta 40× NA 1.4 lens; Carl Zeiss MicroImaging Inc., Tokyo, Japan).

Colorimetric detection of BlaM activity

Transfected 293T cells grown in 6 cm dishes were lysed in 500 μl of buffer A (10 mM HEPES, 1.5 mM $MgCl_2$, 10 mM KCl and 0.05% IGEPAL CA-630), and then 1 μl of nitrocefin (10 μg ml^{-1}; Calbiochem, San Diego, CA, USA) was added to the cell lysate. The mixture was incubated for 20 min at 37 °C.

Protein transduction

The pseudoinfection was performed as infecting cells with retroviral vectors[20] by incubating ~1×10^6 cells with 1 ml LENA-containing culture medium at 37 °C for 1–3 h in the presence of dextran (final concentration 16.25 μg ml^{-1}; DEAE-Dextran chloride, molecular weight ~500 kDa; ICN Biomedicals Inc., Aurora, OH, USA). The cells were assayed by flow cytometry or fluorescent microscopy after the LENA exposure. Bafilomycin A1 was purchased from Sigma.

Fluorescent detection of BlaM activity

A fluorescence-activated cell sorter Aria (Becton Dickinson, San Jose, CA, USA) was used to detect the CCF2-AM (Invitrogen) signals from 293T cells. A violet 407 nm laser was used for fluorescence activation, and BP450/40 nm and LP502 in conjunction with BP530/30 filters were used for the fluorescent signal detection of cleaved and uncleaved substrates, respectively. The CCF2-AM signals from 293T and MT-4 cells were imaged by Biorevo (BZ-9000, Keyence, Osaka, Japan) using the blue filter set (excitation, band pass filters 377/50 nm wavelength; emission, band pass 447/60 nm wavelength; dichroic mirror, 409 nm wavelength) and the green filter set (excitation, band pass filters 377/50 nm wavelength; emission, band pass 520/35 nm wavelength; dichroic mirror, 495 nm wavelength).

CONFLICT OF INTEREST

The authors declare no conflict of interest.

ACKNOWLEDGEMENTS

This work was supported by the Japan Health Science Foundation, the Japanese Ministry of Health, Labor, and Welfare (H18-AIDS-W-003 to JK) and the Japanese Ministry of Education, Culture, Sports, Science and Technology (18689014 and 18659136 to JK).

1 MacGregor RR. Clinical protocol. A phase 1 open-label clinical trial of the safety and tolerability of single escalating doses of autologous CD4 T cells transduced with VRX496 in HIV-positive subjects. *Hum Gene Ther* 2001; **12**: 2028–2029.
2 Cockrell AS, Kafri T. Gene delivery by lentivirus vectors. *Mol Biotechnol* 2007; **36**: 184–204.
3 McCart JA, Bartlett DI. Lentiviral Vectors. In: Templeton NS (ed.). *Gene and Cell Therapy: Therapeutic Mechanisms and Strategies*, 3rd edn. CRC Press: Carrollton, 2008, pp 245–262.
4 Lundberg C, Björklund T, Carlsson T, Jakobsson J, Hantraye P, Déglon N *et al.* Applications of lentiviral vectors for biology and gene therapy of neurological disorders. *Curr Gene Ther* 2008; **8**: 461–473.
5 Jacks T, Power MD, Masiarz FR, Luciw PA, Barr PJ, Varmus HE. Characterization of ribosomal frameshifting in HIV-1 gag-pol expression. *Nature* 1988; **331**: 280–283.
6 Klein KC, Reed JC, Lingappa JR. Intracellular destinies: degradation, targeting, assembly, and endocytosis of HIV Gag. *AIDS Rev* 2007; **9**: 150–161.
7 Briggs JA, Simon MN, Gross I, Kräusslich HG, Fuller SD, Vogt VM *et al.* The stoichiometry of Gag protein in HIV-1. *Nat Struct Mol Biol* 2004; **11**: 672–675.
8 Wyma DJ, Jiang J, Shi J, Zhou J, Lineberger JE, Miller MD *et al.* Coupling of human immunodeficiency virus type 1 fusion to virion maturation: a novel role of the gp41 cytoplasmic tail. *J Virol* 2004; **78**: 3429–3435.
9 Urano E, Aoki T, Futahashi Y, Murakami T, Morikawa Y, Yamamoto N *et al.* Substitution of the myristoylation signal of human immunodeficiency virus type 1 Pr55Gag with the phospholipase C-delta1 pleckstrin homology domain results in infectious pseudovirion production. *J Gen Virol* 2008; **89**: 3144–3149.
10 Aoki T, Shimizu S, Urano E, Futahashi Y, Hamatake M, Tamamura H *et al.* Improvement of lentiviral vector-mediated gene transduction by genetic engineering of the structural protein Pr55(Gag). *Gene Therapy* 2010; **17**: 1124–1133.
11 Voelkel C, Galla M, Maetzig T, Warlich E, Kuehle J, Zychlinski D *et al.* Protein transduction from retroviral Gag precursors. *Proc Natl Acad Sci USA* 2010; **107**: 7805–7810.
12 Hubner W, Chen P, Del Portillo A, Liu Y, Gordon RE, Chen BK. Sequence of human immunodeficiency virus type 1 (HIV-1) Gag localization and oligomerization monitored with live confocal imaging of a replication-competent, fluorescently tagged HIV-1. *J Virol* 2007; **81**: 12596–12607.
13 Campbell RE. Realization of beta-lactamase as a versatile fluorogenic reporter. *Trends Biotechnol* 2004; **22**: 208–211.
14 Wagner R, Graf M, Bieler K, Wolf H, Grunwald T, Foley P *et al.* Rev-independent expression of synthetic gag-pol genes of human immunodeficiency virus type 1 and simian immunodeficiency virus: implications for the safety of lentiviral vectors. *Hum Gene Ther* 2000; **11**: 2403–2413.
15 Ulett GA, Han S, Han JS. Electroacupuncture: mechanisms and clinical application. *Biol Psychiatry* 1998; **44**: 129–138.
16 Ford KG, Souberbielle BE, Darling D, Farzaneh F. Protein transduction: an alternative to genetic intervention? *Gene Therapy* 2001; **8**: 1–4.
17 Zhang Y, Yu LC. Microinjection as a tool of mechanical delivery. *Curr Opin Biotechnol* 2008; **19**: 506–510.
18 Cavrois M, De Noronha C, Greene WC. A sensitive and specific enzyme-based assay detecting HIV-1 virion fusion in primary T lymphocytes. *Nat Biotechnol* 2002; **20**: 1151–1154.
19 Yamanaka S, Blau HM. Nuclear reprogramming to a pluripotent state by three approaches. *Nature* 2010; **465**: 704–712.
20 Komano J, Miyauchi K, Matsuda Z, Yamamoto N. Inhibiting the Arp2/3 complex limits infection of both intracellular mature vaccinia virus and primate lentiviruses. *Mol Biol Cell* 2004; **15**: 5197–5207.
21 Stauffer TP, Ahn S, Meyer T. Receptor-induced transient reduction in plasma membrane PtdIns(4,5)P2 concentration monitored in living cells. *Curr Biol* 1998; **8**: 343–346.
22 Miyauchi K, Komano J, Yokomaku Y, Sugiura W, Yamamoto N, Matsuda Z. Role of the specific amino acid sequence of the membrane-spanning domain of human immunodeficiency virus type 1 in membrane fusion. *J Virol* 2005; **79**: 4720–4729.

Regulation of the susceptibility of HIV-1 to a neutralizing antibody KD-247 by nonepitope mutations distant from its epitope

Mari Takizawa[a], Kosuke Miyauchi[a], Emiko Urano[a], Shigeru Kusagawa[a], Katsuhiko Kitamura[b], Satoshi Naganawa[c], Toshio Murakami[d], Mitsuo Honda[e], Naoki Yamamoto[f] and Jun Komano[a]

Objective: A humanized neutralizing antibody, KD-247, targets the V3 loop of HIV-1 Env. HIV-1 bearing the GPGR sequence at the V3 loop is potentially susceptible to KD-247. However, not all GPGR-positive HIV-1 isolates are neutralized by KD-247. We examined the potential mechanism by which the susceptibility of HIV-1 to KD-247-mediated neutralization is regulated.

Design: We searched for nonepitope neutralization regulatory (NNR) mutations that sensitize GPGR-bearing HIV-1_{AD8} to KD-247 and mapped the locations of such mutations relative to the V3 loop.

Methods: We generated a functional HIV-1_{AD8} Env library, and evaluated the viral susceptibility to KD-247 by measuring the half-inhibitory concentration (IC_{50}) to KD-247 on TZM-bl cell assay.

Results: We identified nine KD-247-sensitizing NNR mutations from 30 mutations in various regions of gp120, including the V1/V2 loop, C2, V3 loop, C4, and C5. They specifically affected KD-247-mediated neutralization, as they did not affect the b12-mediated neutralization. When combined, the KD-247-sensitizing NNR mutations additively sensitized the virus to KD-247 by up to 10 000 folds. The KD-247-sensitizing NNR mutations increased KD-247 binding to the virion. Notably, the NNR mutation in C4 coincides with the CD4-binding site of gp120.

Conclusion: Given that most of the KD-247-sensitizing NNR mutations are remote from V3 loop, it is reasonable to hypothesize that the steady-state, local conformation of the V3 loop is regulated by the interdomain contact of gp120. Our mutational analysis complements crystallographic studies by helping provide a better understanding of the steady-state conformation and the functional geometry of Env.

AIDS 2011, **25**:2209–2216

Keywords: envelope, HIV-1, KD-247, neutralization, steady-state conformation

Introduction

HIV-1 is a highly mutagenic virus. The viral envelope glycoprotein gp120/41 (Env) accumulates mutations to escape from the host humoral immunity. The study on HIV-1-neutralizing antibodies (Nabs) and the viral escape from Nab gives us insights into viral pathogenesis, structure–function relationship of Env, and AIDS vaccine design [1–8].

[a]AIDS Research Center, National Institute of Infectious Diseases, Tokyo, [b]Department of Public Health, Yokohama City University School of Medicine, Yokohama, [c]Infectious Disease Regulation Project, The Tokyo Metropolitan Institute of Medical Science, Tokyo, [d]The Chemo-Sero-Therapeutic Research Institute, Kumamoto, [e]Department of Pathology and Microbiology, Division of Microbiology, Nihon University School of Medicine, Tokyo, Japan, and [f]Department of Microbiology, Yong Loo Lin School of Medicine, National University of Singapore, Singapore.

Correspondence to Jun Komano, AIDS Research Center, National Institute of Infectious Diseases, 1-23-1 Toyama Shinjuku, Tokyo 162-8640, Japan.

Tel: +81 3 5285 1111; fax: +81 3 5285 5037; e-mail: ajkomano@nih.go.jp

Received: 8 September 2010; revised: 4 July 2011; accepted: 5 August 2011.

DOI:10.1097/QAD.0b013e32834bab68

ISSN 0269-9370 © 2011 Wolters Kluwer Health | Lippincott Williams & Wilkins

A humanized monoclonal Nab, KD-247, which is effective against half of clade B primary HIV-1 isolates, targets the third hypervariable (V3) loop, is an attractive AIDS vaccine target [1–3]. The epitope essential for KD-247-mediated neutralization is the conserved tetrapeptide sequence GPGR (HXB2 coordinate 312–315). A human monoclonal Nab 447–52D targets this same epitope [4]. Mutations in the GPGR sequence confer viral resistance to KD-247 [3,5,6]. Moreover, amino acid changes adjacent to the GPGR motif have also conferred viral resistance to KD-247 (e.g. H, R, and K at 311 position, or P at 316 position) [3]. Such mutations physically interfere with binding to the KD-247 epitope [3]. In the absence of such mutations, HIV-1 bearing the GPGR sequence at the V3 loop is potentially susceptible to KD-247. However, not all GPGR-positive HIV-1 isolates are neutralized by KD-247. The mechanism by which some of the GPGR-bearing viruses are resistant to KD-247 is not fully understood.

We addressed this sequence-neutralization susceptibility discordance by comparing the amino acid sequences of various HIV-1 primary isolates. We defined a virus as resistant to KD-247-mediated neutralization when the half-inhibitory concentration (IC_{50}) was higher than 100 μg/ml. We analyzed V3 loop amino acid sequences from 25 viruses positive for the GPGR epitope, including 11 KD-247-sensitive and 14 KD-247-resistant viruses. Along with the ELISA data in our previous report [3], we found that H304R contributes to KD-247 resistance. The H304R polymorphism accounted for 35.7% (five of 14 isolates) of the examples of sequence-neutralization susceptibility discordance, but all the viruses carrying H304R were CRF01_AE. We failed to identify any neutalization regulatory mutations in the clade B isolates. Additionally, the KD-247 prototype mouse monoclonal antibody C25 was unable to neutralize 17 GPGR-positive HIV-1 clade B primary isolates, even though C25 was able to bind their synthetic V3 loop peptides (unpublished observation). From these data, we postulated that the sequence-neutralization susceptibility discordance is due to non-epitope neutralization regulatory (NNR) mutations, especially remote from the V3 loop. Such NNR mutations would be positioned at certain key sites within the Env domains and regulate the steady-state conformation. NNR mutations have been predicted for 447–52D and other cross-reactive Nab [6–11]. To test this hypothesis, we examined 15 entire Env amino acid sequences of KD-247-sensitive and KD-247-resistant viruses. However, we were unable to identify amino acids associated with susceptibility to KD-247. This suggests that the heterologous virus approach is not sensitive enough to identify NNR mutations because the diversity of Env amino acid sequences is beyond the level of detection.

Here we employed a genetic approach to identify NNR mutations using the HIV-$1_{AD8/ADA}$ (AD8 hereafter), which displays the sequence-neutralization susceptibility discordance. The AD8 strain has been reported to be sensitive to 447–52D, which targets the same neutralization epitope as KD-247 within the V3 loop [10], suggesting that the GPGR epitope of the V3 loop is open to antibodies. We thought that this should help understand how the NNR mutations work. It does not contain insertions adjacent to the GPGR motif, as HIV-1_{HXB2} or HIV-1_{NL4-3} do (QR insertion before I and G) nor H304R. Only a few NNR mutations that make HIV-1 resistant to KD-247 have been reported in the V1/V2 loop [6]. In this work, we generated a functional AD8 Env library to identify many NNR mutations simultaneously that cause HIV-1 to become susceptible to KD-247. Through KD-247-sensitizing NNR mutations, we tried to understand the regulatory mechanism of the viral susceptibility to KD-247-mediated neutralization.

Materials and methods

Cells, viruses, and transfection

Cells were maintained in RPMI-1640 Medium (Sigma, St Louis, Missouri, USA) supplemented with 10% fetal bovine serum (FBS) (Japan Bioserum, Tokyo, Japan), 50 U/ml penicillin, and 50 μg/ml streptomycin (Invitrogen, Tokyo, Japan), at 37°C in a humidified 5% CO_2 atmosphere. Cells were transfected with Lipofectamine 2000 according to the manufacturer's protocol (Invitrogen). The other viruses and TZM-bl cells were obtained from the NIH AIDS Research and Reference Reagent Program.

Antibodies

KD-247 was provided by the Chemo-Sero-Therapeutic Research Institute, and b12 is a generous gift from Dr Burton (The Scripps Research Institute).

Cloning

AD8 Env was amplified by nested reverse-transcriptase-PCR using RNA extracted from the culture supernatant as a template (RNeasy mini kit; Qiagen, Hilden, Germany). The primers used were as follows. For the first PCR, the sense primer was 5′-ATG AAA CTT ACG GGG ATA CTT GGG-3′ (HXB2 nucleotide coordinates 5698–5721) and the antisense primer was 5′-GGT ACT AGC TTG AAG CAC CAT CC-3′ (HXB2 nucleotide coordinates 9236–9214); and for the nested PCR, the sense primer was 5′-ATA AGA ATT CTG CAA CAA CTG CTG-3′ (HXB2 nucleotide coordinates 5739–5762) and the antisense primer was 5′-TTC CAG GTC TCG AGA TGC TGC-3′ (HXB2 nucleotide coordinates 8910–8890). EcoRI-XhoI fragments of the PCR products were cloned into the corresponding restriction sites of pNL4–3. The *env* gene was sequenced using the following primers: 3479a, 5′-CTT GGG ATG TTG

ATG ATC TGT AGT GCT GTA GA-3′; 003A, 5′-AGC AGA AGA CAG TGG CAA TG-3′; 106A, 5′-CAT ACA TTA TTG TGC CCC GGC TGG-3′; 545A, 5′-GAC AAT TGG AGA AGT GAA TT-3′; and 5700, 5′-AGC CTG TGC CTC TTC AGC TAC CAC CGC TTG-3′.

Neutralization assay

To produce virus from proviral DNA, 293FT cells (Cat# R700–007; Invitrogen) grown in six-well plates were transfected with proviral DNA-encoding plasmid (1 μg) using Lipofectamine 2000, and replated into a six-well plate at 4–6 h posttransfection. At 48 h posttransfection, the cell culture medium was collected and mixed with dextran (final concentration 16.25 μg/ml, DEAE-Dextran chloride, molecular weight ~500 kDa; ICN Biomedicals Inc., Aurora, Ohio, USA). The TZM-bl cells were plated in 96-well plates at 500 cells per well in a volume of 100 μl a day before infection. The virus and KD-247 were mixed in a volume of 50 μl and incubated at 37°C for 30 min. Then, the TZM-bl cells were exposed to the virus-KD-247 mixture. At 3 days postinfection, luciferase activity was measured using the Steady-Glo Luciferase Assay system (Promega, Madison, Wisconsin, USA). The IC_{50} was defined as the Nab concentration that yielded a half-reduction in luciferase activity compared with the control wells after subtracting background signals as previously described [12]. Luminescence was detected using a Veritas Microplate Luminometer (Promega). The GHOST cell-based and peripheral blood mononuclear cell-based neutralization assays were performed as described previously [3].

Virus capture ELISA

The ELISA plate (Nunclon, Roskilde, Denmark) was coated by KD-247 with incubating plates with 100 μl of KD-247 preparation (10 μg/ml) in a carbonate buffer (15 mmol/l Na_2CO_3, 35 mmol/l $NaHCO_3$, pH 9.6) at 4°C overnight. Plates were washed five times with Plate Wash Buffer (Zeptometrics, Buffalo, New York, USA), and blocked with PBS containing 20% FBS (Nalgene, Rochester, New York) at 37°C for 1 h. After washing the plates for five times with Plate Wash Buffer and once with PBS, virus was captured by KD-247 by incubating plates with viral preparations containing 50 ng of $p24^{CA}$ resuspended in a volume of 100 μl PBS. After washing PBS with 10% FBS, captured virus was lysed in a buffer and a $p24^{CA}$ ELISA was conducted according to the manufacturer's protocol (Zeptometrics).

Results

Construction of a functional Env library based on the AD8 strain

In theory, it is possible to identify NNR mutations conferring viral resistance to the Nab by selecting Nab-resistant mutants from a Nab-sensitive virus in culture. However, this approach is not ideal for the identification of many NNR mutations at the same time because it primarily selects epitope mutants and only a few dominant NNR mutants. To overcome this problem, we tried to identify NNR mutations that sensitize HIV-1 to KD-247. To achieve this goal, we generated a functional Env library and tried to identify KD-247-sensitizing NNR mutations by correlating mutations with viral susceptibility to KD-247-mediated neutralization. We chose a KD-247-resistant strain, AD8, that shows sequence-neutralization susceptibility discordance, and its IC_{50} to KD-247, when the virus is produced in 293T cells from a proviral DNA, was 354.9 μg/ml by TZM-bl assay (average of five independent experiments). Interestingly, this strain has been reported to be sensitive to 447–52D, which targets the same neutralization epitope within the V3 loop [10]. This suggests that the GPGR epitope of the V3 loop is open to antibodies, and the hindrance of KD-247 epitope is unlikely.

An Env mutant library can be produced by genetic engineering (e.g., PCR-based random mutagenesis). However, such an approach does not always produce functional Env. In contrast, Env mutants generated by viral diversification in tissue culture should be functional unless sporadic mutations that interfere with Env function are introduced. We took the latter approach to generate a functional Env library. We diversified AD8 viruses by approximately 100 passages in MOLT-4 cells. This was a simple bulk passage of virus, whereby tissue culture supernatant was transferred to fresh cells, likely conferring the survival of random mutations. We examined the diversity by sequencing 56 *env* clones. Of these 56 clones, 54 *env* clones were independent, suggesting that the diversification of *env* was successful. The IC_{50} of diversified AD8 to KD-247 was 334.6 μg/ml by TZM-bl assay (average of three independent experiments), suggesting that the diversified AD8 is resistant to KD-247 when scored in bulk. Our data indicate that long-term viral selection in tissue culture does not necessarily select a few dominant mutants; various mutants of independent origins can be maintained. We expected that most of the amino acid substitution mutations should not damage Env function; otherwise, they should not have been selected in culture. The average number of mutations was 3.0 per clone, including the frameshift and stop codon mutations, and, importantly, every virus retained the GPGR epitope in the V3 loop. These viruses were distinct from each other but not as divergent as a panel of field isolates, making them suitable for the identification of KD-247-sensitizing NNR mutations. Our diversification protocol does not necessarily select Env mutants with higher or lower susceptibility to KD-247. We expect that some (but not all) mutations may increase the susceptibility to KD-247. We next evaluated whether any mutations could confer the increased susceptibility of the AD8 strain to KD-247.

Identification of nonepitope neutralization regulatory mutations in various domains of gp120

In our viral diversification protocol, mutations can occur in any region of the viral genome. We are concerned that non-Env mutations could affect neutralization susceptibility to KD-247. For example, the IC_{50} could be scored lower if the viral fitness is poor and higher if viral fitness is high. To avoid these possibilities, we cloned diversified Env into the same viral genetic background. We chose HIV-1_{NL4-3} because it is one of the standard molecular clones of HIV-1, and the proviral DNA is relatively stable and, thus, suitable for such cloning. The AD8 *env* cloned HIV-1_{NL4-3} was named NL/AD8. At first, we verified that the susceptibility of viral isolates to KD-247-mediated neutralization could be reproduced on the HIV-1_{NL4-3} genetic background. For this purpose, we used HIV-1_{MN} and AD8 Env, which are highly susceptible and resistant to KD-247, respectively. Cloning *env* from KD-247-sensitive HIV-1_{MN} into HIV-1_{NL4-3} reproduced neutralization susceptibility (IC_{50} 0.07 μg/ml). Similarly, the KD-247 resistance seen in the AD8 strain was reproduced in the NL/AD8 viruses (IC_{50} 357.5 μg/ml, Table 1). Env mutants with no stop codon or frameshift were tested on the HIV-1_{NL4-3} background. Chimeric viruses carrying AD8 Env mutants that did not yield and infectivity index in TZM-bl cells comparable to that of viruses carrying NL4–3/AD8 were not tested further. Viruses bearing combinations of mutations were generated by positioning mutations between useful restriction enzyme recognition sites in the viral genome. Finally, we examined 27 molecular clones by substituting HIV-1_{NL4-3} *env* with the diversified AD8 *env* clones or AD8 *env* with a point mutation found in the diversified pool (Table 1) Mutations causing Env amino acid changes did not comutate the viral proteins encoded in the Env-overlapping frames including *vpu, tat*, and *rev*.

We determined the IC_{50} of KD-247 on these viruses using TZM-bl cells. Out of 27 viruses, 19 increased their susceptibility to KD-247-mediated neutralization to more than two-fold that of NL/AD8 (19 of 27 clones, 70.4%; Table 1), consistent with previous reports suggesting that the long-term passages *in vitro* select Nab-susceptible HIV-1 [13,14]. Comparing the IC_{50} for each of the mutations, we identified nine NNR mutations that sensitized viruses to KD-247 by more than two-fold (nine of 30 mutations, 30.0%; Table 2). A mutation that altered the IC_{50} no more than two-fold was defined as a non-NNR mutation. Seventeen

Table 1. Summary of half-inhibitory concentration of mutant viruses against KD-247 and b12.

	KD-247		b-12	
Mutations[a]	IC_{50} (μg/m)[b]	Fold sensitization[c]	IC_{50} (μg/m)[b]	Fold sensitization[c]
NL/AD8	357.5 ± 121.8	1	2.4 ± 1.0	1
T48A, D163N, R248M, N297S, S370N, A721T	0.03 ± 0.02	12 342.2	0.2 ± 0.1	12.6
T48A, S186R, S302G S370N, F764S*	7.0 ± 5.5	50.8	0.7 ± 0.2	3.3
S370N, K428E, Q504R, A509T, G689S	39.8 ± 25.9	9.0	1.0 ± 0.3	2.3
D163G, R300G, S370N, S760G	4.4 ± 3.9	82.1	0.4 ± 0.1	6.0
K285R, N298Y, I488T, E506K	480.9 ± 27.1	0.7	1.8 ± 1.1	1.3
E31G, T48A, N279T	141.4 ± 53.1	2.5	1.0 ± 0.2	2.5
D181G, N298Y, S760G	350.0 ± 173.2	1.0	1.8 ± 0.9	1.3
S186R, S370N, S760G	102.8 ± 8.1	3.5	NT	
N298Y, S370N, S760G	380.9 ± 70.7	0.9	1.9 ± 1.0	1.3
V178A, N298Y	89.0 ± 29.3	4.0	8.7 ± 0.9	0.3
N191D, N298Y	157.2 ± 76.8	2.3	1.5 ± 0.9	1.6
I280M, S370N	284.6 ± 34.3	1.3	6.4 ± 0.5	0.4
N297S, S370N	2.4 ± 1.8	149.0	0.8 ± 0.2	3.0
N298Y, E655G*	428.1 ± 47.5	0.8	1.1 ± 0.0	2.3
S370N, N391S	280.5 ± 29.6	1.3	2.5 ± 1.9	1.0
S370N, I546V	303.6 ± 60.8	1.2	2.0 ± 0.2	1.2
S370N, A580T	81.3 ± 18.0	4.4	2.6 ± 0.7	0.9
D163G	6.0 ± 3.5	59.4	1.3 ± 0.0	1.9
D163N	4.8 ± 2.4	74.3	0.9 ± 0.4	2.6
S186R	46.7 ± 24.4	7.7	1.0 ± 0.3	2.4
R248M	59.7 ± 35.8	6.0	2.6 ± 0.7	0.9
N297S	3.0 ± 1.4	119.2	1.2 ± 0.5	2.1
R300G	68.8 ± 28.1	5.2	2.2 ± 1.2	1.1
S302G	6.6 ± 3.4	54.4	2.2 ± 1.1	1.1
S370N	211.5 ± 92.1	1.7	1.2 ± 0.5	2.0
K428E	39.3 ± 35.0	9.1	2.1 ± 0.1	1.2
Q504R	121.6 ± 38.5	2.9	2.7 ± 1.0	0.9

IC_{50}, half-inhibitory concentration; NT, not tested.
[a]NL/AD8 was used as a reference. The amino acid numbering is according to HIV-1AD8 Env. The virus without an asterisk was subjected to virus–antibody binding experiment shown in Fig. 1.
[b]The average and SD from two to 13 independent experiments are shown.
[c]The IC_{50} of the control virus was divided by IC_{50} of each mutant.

Table 2. Summary of mutations characterized in this study.

Mutations[b]	HXB2 coordinate	Location in Env[a]	Fold sensitization
NNR			
D163G	G167	V1/V2	59.4
D163N	G167	V1/V2	74.3
S186R	K192	V1/V2	7.7
R248N	R252	C2	7.0
N297S	N301	V3	119.2
R300G	R304	V3	5.2
S302G	R306	V3	54.4
K428E	K432	C4	9.1
Q504R	Q507	C5	2.9
Non-NNR			
E31G[c]	E32	C1	–
T48A[c]	T49	C1	–
V178A[c]	I181	V1/V2	–
D181G	D185	V1/V2	–
N191D[c]	S195	V1/V2	–
K285R	N289	V3	–
N298Y	N302	V3	–
S370N	S375	C3	–
N391S	X396	V4	–
I488T	I491	C5	–
E506K	E509	C5	–
A509T[c]	A512	gp41	–
I546V	I548	gp41	–
A580T[c]	A582	gp41	–
E655G	E657	gp41	–
G689S[c]	G691	gp41	–
S760G	S762	gp41	–

NNR, nonepitope neutralization regulatory.
[a]The gp120 was subdivided into C1, V1/V2, C3, V3, C4, V4, and C5.
[b]NNR mutations conferring a change in neutralization susceptibility of more than two-fold. Non-NNR mutations are defined as mutations conferring a change in neutralization susceptibility of no more than two-fold.
[c]Estimated from the fold sensitization of a mutant carrying multiple mutations.

non-NNR mutations were also found (Table 2). The magnitude of sensitization by NNR mutations ranged from 2.9 to 119.2. These NNR mutations were present in a broad range of gp120 sites, including V1/V2 loop, C2, V3 loop, C4, and C5. When combined, the NNR mutations additively sensitized the virus to KD-247 by up to 10 000-fold, suggesting an independent structural cross-talk between the V3 loop and each NNR mutation. Such a drastic effect was not observed against b12 Nab targeting the CD4-binding site of gp120 (Table 1). The effect of these NNR mutations appeared to be specific to KD-247, as evidenced by the statistically insignificant correlation between IC_{50} values for KD-247 and b12 (Supplementary Information S1, http://links.lww.com/QAD/A180). This is probably due to the conserved nature of the b12 epitope structure and function. It should be noted that infection with mutant viruses yielded similar levels of luciferase signal from TZM-bl cells when comparable amounts of viruses were used. Also, the viruses bearing six mutations (T48A, D163N, R248M, N297S, S370N, and A721T) replicated in MOLT-4/CCR5 cells with similar efficiency to the no mutation control (NL/AD8), suggesting that replication competency can not account for the change in neutralization susceptibility (data not shown).

Correlation between neutralization susceptibility and KD-247 binding affinity to the virion

We investigated how NNR mutations could sensitize a virus to KD-247-mediated neutralization. We tested whether the KD-247-sensitizing NNR mutation could induce a conformational change in gp120 in such a way that KD-247 became able to bind to gp120 with higher efficiency. To address this question, we performed a capture ELISA in which ELISA plates were precoated with KD-247 and blocked, followed by incubation of virions bearing NNR mutations in the wells of the ELISA plate. The amount of KD-247 captured virus was quantified by ELISA detecting the viral core antigen (Fig. 1). If the latter model is correct, KD-247 captures every mutant with similar efficiencies. As a result, viral binding to KD-247 was significantly correlated with neutralization susceptibility ($P < 0.01$, $n = 26$, two-tailed Student's *t*-test; Fig. 1). These data support a model in which KD-247-sensitizing NNR mutations alter the steady-state structure of gp120 into a conformation such that KD-247 is able to bind to its target with higher efficiencies.

Structural analysis of nonepitope neutralization regulatory mutations

To gain insight into the potential mechanisms whereby KD-247-sensitizing mutations enable neutralization of virions, we used the three-dimensional structural model described by Blay *et al.* [15]. We used an X-ray crystallographic structure with variable loops [15], which was aligned in a trimeric form in accordance with a model developed by Pancera *et al.* [16].

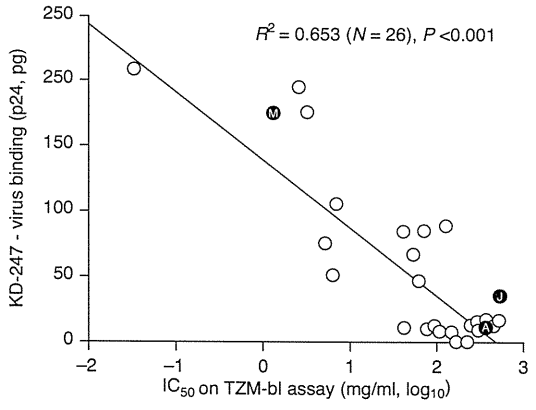

Fig. 1. Analysis of neutralization susceptibility of HIV-1 to KD-247. The half-inhibitory concentration (IC_{50}) for each virus for KD-247 is plotted against the virus capture ELISA data using KD-247 as summarized in Table 1. A significant correlation between the two parameters was detected ($P < 0.01$, two-tailed Student's *t*-test). HIV-1_{MN}, HIV-1_{JR-FL}, and HIV-$1_{NL/AD8}$ are shown as M, J, and A, respectively.

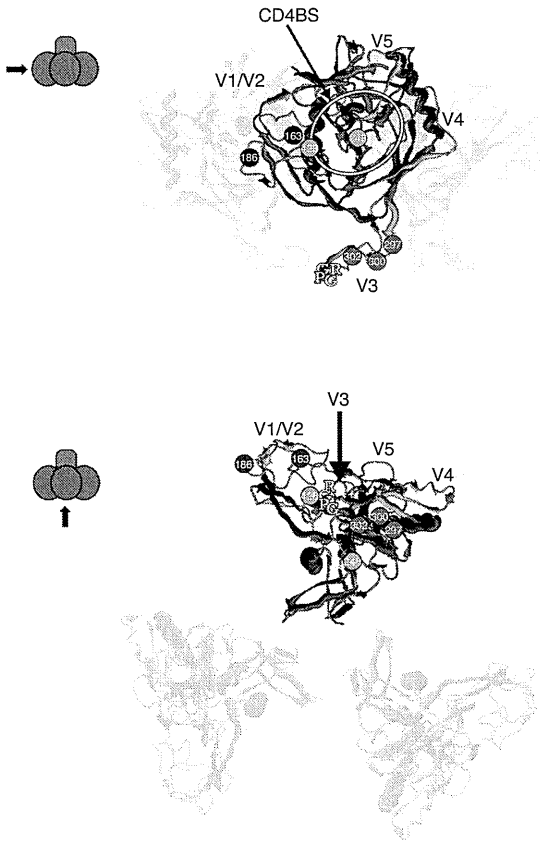

Fig. 2. The three-dimensional mapping of KD-247-sensitizing non-epitope neutralization regulatory mutations based on the Env structure aligned in a trimeric form. The view angle is indicated on the left (arrows) where the gp120 and gp41 are shown in sphere (purple) and rectangle (red), respectively. The gp120 core was shown in blue and red, and the variable loops are shown in yellow. KD-247-sensitizing non-epitope neutralization regulatory (NNR) mutations are indicated by their amino acid numbers. The NNR mutations on the V1/V2 loop, V3 loop, and gp120 core are shown in blue, red, and green, respectively. The GPGR on the V3 loop is shown as a letter code in yellow. The approximate CD4-binding site (CD4BS) is indicated by a white line. The original structural image was developed by Blay *et al.* [15]

The R248N in the C2 region is placed on the gp41 side of the gp120 surface and is not facing the trimeric interface of gp120 (Fig. 2, green) [15]. It has been reported that the H66N, positioned near the trimeric interface of gp120, induces a conformational change of gp120 [17,18]. It has been proposed that H66N alters the quaternary Env structure by acting intermolecularly rather than intramolecularly. In contrast to H66N, the R248N is not positioned at or close to the trimeric surface of gp120. It is likely that R248N induces a different conformational change of the gp120 from H66N, one that does not affect the neutralization susceptibility to b12. It is of interest that the remote KD-247-sensitizing NNR mutation of the gp120 core can specifically affect the conformation of the V3 loop positioned on the gp120 surface.

K428E in the C4 region was mapped in the CD4-binding site close to the so-called bridging sheet (Fig. 2, green), suggesting that the V3 loop and CD4-binding site neutralization epitopes can influence each other's conformation under steady-state conditions. Like R248N, K428E is not positioned at or close to the gp120 trimeric interface. Thus, we speculate that K428E induces a local, not global, Env conformational change. The amino acid corresponding to K428 has been implicated previously in b12 binding through its side-chain as well as through CD4, using HXBc2 Env as a model [19,20]. K428E induces a drastic change in side-chain properties. However, K428E did not significantly affect the viral susceptibility to b12 and the replication efficiency of the NL/AD8 backbone, suggesting that this amino acid may not play a significant role in AD8 Env–b12 interaction. K428 is positioned at the edge of the b12–Env or CD4–Env contact region and, thus, may not contribute significantly to b12–Env or CD4–Env interaction in the context of AD8 Env. Structural cross-talk between the V3 loop and the C4 region under steady-state conditions has been suggested by two studies using monoclonal antibodies. Our approach pinpointed the amino acids responsible for this inter-domain cross-talk.

In contrast to the above two mutations, the precise positioning of KD-247-sensitizing NNR mutations in the V1/V2 and V3 loop is unclear because structural information for them are lacking in the original crystallographic data. According to the molecular dynamics modeling [15], the KD-247-sensitizing NNR mutations in the V1/V2 and V3 loop may not be positioned at or close to the trimeric surface of gp120 (Fig. 2). Instead, they function intramolecularly to affect the conformation of the KD-247 epitope. The Q504R is also lacking in the X-ray crystal structures. However, Q504R is next to the gp120/41 cleavage site and should be close to gp41. The gp41 is relatively proximal to the CD4-binding site of gp120. Some of the mutations in gp41, including T569A and I675V, have been reported to influence the viral susceptibility to Nabs, including b12 [21]. It is conceivable that these mutations in gp41 affect the conformation of gp120. In contrast to T569A and I675V, Q504R is not a b12-sensitizing NNR mutation. Therefore, the conformational change of gp120 induced by Q504R should be distinct from the gp41 mutations.

The structural approach has a potential limitation because the molecular model of Env does not represent the native structure but the liganded structure (Fig. 2). In fact, almost all of the deposited X-ray crystallographic structures are devoid of V1/V2 and/or V3 loops and do not represent the native Env structure, including

the model that our figure is built upon [4,8,15,16,19,22–24].

Discussion

In this work, we identified a number of KD-247-sensitizing NNR mutations using a functional Env library. We re-examined KD-247-sensitive or KD-247-resistant GPGR-positive HIV-1 isolates for NNR mutations and found that KD-247-sensitive viruses, MN (a tissue culture adapted strain of MN) and MNp (a primary HIV-1 isolate), had the mutation equivalent to N301S [25,26]. The predictive value for KD-247 susceptibility due to this mutation was high in the clade B population. However, this does not apply to CRF01_AE, suggesting that this mutation is a clade B-specific predictor of viral susceptibility to KD-247. The other KD-247-sensitizing NNR mutations identified in AD8 did not fully account for the neutralization susceptibility of all of the HIV-1 primary isolates. This suggested that additional NNR mutations should be present, and/or NNR mutations in a given individual virus may function differently than in the other viruses.

How do these mutations alter the conformation of Env to increase the susceptibility of virus to KD-247-mediated neutralization? AD8 is originally resistant to KD-247. One of the molecular mechanisms of AD8 resistance to KD-247 is an epitope-masking by other gp120 domains, possibly the V1/V2 loop or polysaccharides attached to the gp120 [6,27]. Recently, however, Gorny *et al.* [28] reported that the V3 loop of AD8 Env is accessible to KD-247, as AD8 is susceptible to 447–52D-mediated neutralization. This clearly suggests that the sensitization of AD8 strain to KD-247 by the NNR mutations we identified is unlikely due to the removal of the Env domains that physically block antibody access to GPGR epitope. We assume that the V3 loop forms a local conformation in which the neutralization epitope of KD-247 is buried or cannot be recognized by a Nab (local epitope conformation model). When the KD-247-sensitizing NNR mutation occurs, it induces a local, not a global, conformational change of the V3 loop that exposes the neutralization epitope of KD-247. Most of the KD-247-sensitizing NNR mutations are remote from V3 loop. Thus, we assume that KD-247-sensitizing NNR mutations may be located at or close to the interdomain contact regions, and regulate the local conformation of the V3 loop indirectly. Although proven by X-ray crystallographic studies, we propose that the steady-state Env structure is regulated such a way that the domain-independent structural fluctuation is limited. This model predicts that the steady-state structure of the V3 loop is relatively rigid and that its local conformational fluctuation is restricted. This model is relevant to understand the mechanism of action of other NNR mutations against array of Nabs [6–11].

Much attention has been paid to the structural dynamics of HIV-1 Env on CD4 and/or Nab binding. In contrast, not as much attention has been paid to the steady-state conformational dynamics of Env. Unlike previous studies, ours focuses on the steady-state conformational regulation of Env. X-ray crystallography is the best approach to solve a high-resolution native Env structure. However, technical hurdles prevent us from doing so for HIV-1 Env. We examined the mechanism by which the Env conformation is regulated by utilizing Nab KD-247 as a probe. Our approach to identify NNR mutations should complement the crystallization approach in achieving a better understanding of the steady-state structure of HIV-1 Env. Revealing the native structure of Env is critical to the design of an immunogen for the AIDS vaccine and to an understanding of how Env supports virus–cell membrane fusion from the receptor-unbound state.

Acknowledgements

The authors would like to thank Dr Nancy Haigwood for kindly providing the Env structural data. M.T., K.M., E.U., S.K., K.K., S.N., and J.K. designed and performed experiments. T.M., M.H., N.Y., and J.K. analyzed data. J.K. wrote the manuscript.

Conflicts of interest

This work was supported in part by the Japan Health Science Foundation, the Japanese Ministry of Health, Labor and Welfare (H18-AIDS-W-003 and H20-AIDS-G-008 to JK), and the Japanese Ministry of Education, Culture, Sports, Science and Technology (18689014 and 18659136 to J.K.).

There are no conflicts of interest.

References

1. Euler Z, Bunnik EM, Burger JA, Boeser-Nunnink BD, Grijsen ML, Prins JM, *et al.* **Activity of broadly neutralizing antibodies, including PG9, PG16 and VRC01, against recently transmitted subtype B HIV-1 variants from early and late in the epidemic.** *J Virol* 2011; **85**:7236–7245.
2. Hartley O, Klasse PJ, Sattentau QJ, Moore JP. **V3: HIV's switch-hitter.** *AIDS Res Hum Retroviruses* 2005; **21**:171–189.
3. Moore PL, Gray ES, Morris L. **Specificity of the autologous neutralizing antibody response.** *Curr Opin HIV AIDS* 2009; **4**:358–363.
4. Moscoso CG, Sun Y, Poon S, Xing L, Kan E, Martin L, *et al.* **Quaternary structures of HIV Env immunogen exhibit conformational vicissitudes and interface diminution elicited by ligand binding.** *Proc Natl Acad Sci U S A* 2011; **108**:6091–6096.
5. Walker LM, Phogat SK, Chan-Hui PY, Wagner D, Phung P, Goss JL, *et al.* **Broad and potent neutralizing antibodies from an African donor reveal a new HIV-1 vaccine target.** *Science* 2009; **326**:285–289.

6. Walker LM, Burton DR. **Rational antibody-based HIV-1 vaccine design: current approaches and future directions.** *Curr Opin Immunol* 2010; **22**:358–366.
7. Willey S, Aasa-Chapman MM. **Humoral immunity to HIV-1: neutralization and antibody effector functions.** *Trends Microbiol* 2008; **16**:596–604.
8. Zhou T, Georgiev I, Wu X, Yang ZY, Dai K, Finzi A, *et al.* **Structural basis for broad and potent neutralization of HIV-1 by antibody VRC01.** *Science* 2010; **329**:811–817.
9. Wei X, Decker JM, Wang S, Hui H, Kappes JC, Wu X, *et al.* **Antibody neutralization and escape by HIV-1.** *Nature* 2003; **422**:307–312.
10. Gorny MK, Revesz K, Williams C, Volsky B, Louder MK, Anyangwe CA, *et al.* **The v3 loop is accessible on the surface of most human immunodeficiency virus type 1 primary isolates and serves as a neutralization epitope.** *J Virol* 2004; **78**:2394–2404.
11. Gray ES, Moore PL, Bibollet-Ruche F, Li H, Decker JM, Meyers T, *et al.* **4E10-resistant variants in a human immunodeficiency virus type 1 subtype C-infected individual with an antimembrane-proximal external region-neutralizing antibody response.** *J Virol* 2008; **82**:2367–2375.
12. Martin L, Stricher F, Misse D, Sironi F, Pugnière M, Barthe P, *et al.* **Rational design of a CD4 mimic that inhibits HIV-1 entry and exposes cryptic neutralization epitopes.** *Nat Biotechnol* 2003; **21**:71–76.
13. Wrin T, Loh TP, Vennari JC, Schuitemaker H, Nunberg JH. **Adaptation to persistent growth in the H9 cell line renders a primary isolate of human immunodeficiency virus type 1 sensitive to neutralization by vaccine sera.** *J Virol* 1995; **69**:39–48.
14. Zhang YJ, Fredriksson R, McKeating JA, Fenyo EM. **Passage of HIV-1 molecular clones into different cell lines confers differential sensitivity to neutralization.** *Virology* 1997; **238**:254–264.
15. Blay WM, Gnanakaran S, Foley B, Doria-Rose NA, Korber BT, Haigwood NL. **Consistent patterns of change during the divergence of human immunodeficiency virus type 1 envelope from that of the inoculated virus in simian/human immunodeficiency virus-infected macaques.** *J Virol* 2006; **80**:999–1014.
16. Pancera M, Majeed S, Ban YE, Chen L, Huang CC, Kong L, *et al.* **Structure of HIV-1 gp120 with gp41-interactive region reveals layered envelope architecture and basis of conformational mobility.** *Proc Natl Acad Sci U S A* 2010; **107**:1166–1171; Epub 2010 Dec 28..
17. Kassa A, Finzi A, Pancera M, Courter JR, Smith AB 3rd, Sodroski J. **Identification of a human immunodeficiency virus type 1 envelope glycoprotein variant resistant to cold inactivation.** *J Virol* 2009; **83**:4476–4488.
18. Kassa A, Madani N, Schon A, Haim H, Finzi A, Xiang SH, *et al.* **Transitions to and from the CD4-bound conformation are modulated by a single-residue change in the human immunodeficiency virus type 1 gp120 inner domain.** *J Virol* 2009; **83**:8364–8378.
19. Zhou T, Xu L, Dey B, Hessell AJ, Van Ryk D, Xiang SH, *et al.* **Structural definition of a conserved neutralization epitope on HIV-1 gp120.** *Nature* 2007; **445**:732–737.
20. Wu X, Zhou T, O'Dell S, Wyatt RT, Kwong PD, Mascola JR. **Mechanism of human immunodeficiency virus type 1 resistance to monoclonal antibody B12 that effectively targets the site of CD4 attachment.** *J Virol* 2009; **83**:10892–10907.
21. Blish CA, Nguyen MA, Overbaugh J. **Enhancing exposure of HIV-1 neutralization epitopes through mutations in gp41.** *PLoS Med* 2008; **5**:e9.
22. Cho YK, Foley BT, Sung H, Kim YB, Kim JH. **Molecular epidemiologic study of a human immunodeficiency virus 1 outbreak in haemophiliacs B infected through clotting factor 9 after 1990.** *Vox Sang* 2007; **92**:113–120.
23. Huang CC, Tang M, Zhang MY, Majeed S, Montabana E, Stanfield RL, *et al.* **Structure of a V3-containing HIV-1 gp120 core.** *Science* 2005; **310**:1025–1028.
24. Diskin R, Marcovecchio PM, Bjorkman PJ. **Structure of a clade C HIV-1 gp120 bound to CD4 and CD4-induced antibody reveals anti-CD4 polyreactivity.** *Nat Struct Mol Biol* 2010; **17**:608–613.
25. Leavitt M, Park EJ, Sidorov IA, Dimitrov DS, Quinnan GV Jr. **Concordant modulation of neutralization resistance and high infectivity of the primary human immunodeficiency virus type 1 MN strain and definition of a potential gp41 binding site in gp120.** *J Virol* 2003; **77**:560–570.
26. Eda Y, Takizawa M, Murakami T, Maeda H, Kimachi K, Yonemura H, *et al.* **Sequential immunization with V3 peptides from primary human immunodeficiency virus type 1 produces cross-neutralizing antibodies against primary isolates with a matching narrow-neutralization sequence motif.** *J Virol* 2006; **80**:5552–5562.
27. Kwong PD, Wyatt R, Robinson J, Sweet RW, Sodroski J, Hendrickson WA. **Structure of an HIV gp120 envelope glycoprotein in complex with the CD4 receptor and a neutralizing human antibody.** *Nature* 1998; **393**:648–659.
28. Gorny MK, Williams C, Volsky B, Revesz K, Cohen S, Polonis VR, *et al.* **Human monoclonal antibodies specific for conformation-sensitive epitopes of V3 neutralize human immunodeficiency virus type 1 primary isolates from various clades.** *J Virol* 2002; **76**:9035–9045.

PROTEINS
STRUCTURE ■ FUNCTION ■ BIOINFORMATICS

Exploring coumarin egress channels in human cytochrome P450 2A6 by random acceleration and steered molecular dynamics simulations

Weihua Li,[1] Jie Shen,[1] Guixia Liu,[1] Yun Tang,[1]* and Tyuji Hoshino[2]*

[1] Department of Pharmaceutical Sciences, School of Pharmacy, East China University of Science and Technology, Shanghai 200237, China

[2] Graduate School of Pharmaceutical Sciences, Chiba University, Chiba 263-8522, Japan

ABSTRACT

The kinetic analysis of coumarin oxidation by CYP2A6 suggested that substrate binding and release occurred in the multiple steps and such events proceeded rapidly. However, the crystal structure of the CYP2A6-coumarin complex reveals that no obvious channel is open enough to allow coumarin to pass through. Thus, an intriguing and important question arises: how coumarin enters and exits the active site, which is deeply buried at the center of CYP2A6 fold. In this study, geometric analysis of the potential openings was first performed on all the available crystal structures of CYP2A6. And then, random acceleration molecular dynamics simulations were used to explore the possible substrate egress channels in CYP2A6. Two channels were most frequently observed. Afterwards, steered molecular dynamics simulations were performed and potentials of mean force were constructed to compare the preference of the two channels serving as the substrate egress channel. The results showed that channel 2c, which is located between helices I and G and the helix B'-C region, was the most likely channel for coumarin egress. The opening of channel 2c was characterized by a rotation of Phe111 together with a bending of helix B'. Our findings will not only be helpful for understanding the unbinding mechanism of coumarin and for identifying structural determinants related to the biological function of CYP2A6, but also provide further insight into the channel selectivity of P450s.

Proteins 2011; 79:271–281.

Key words: P450 2A6; coumarin; egress channel; molecular dynamics; channel selectivity.

INTRODUCTION

Cytochromes P450 (P450s) are a superfamily of heme-containing monooxygenases that catalyze the metabolism of a large number of endogenous and exogenous compounds, including drugs, environmental pollutants, and carcinogens.[1] In general, P450-mediated metabolism occurs via a catalytic cycle consisting of several steps,[2] including: substrate binding to the active site of P450; reduction of the ferric P450 to the ferrous state by introducing an electron; binding of molecular oxygen to the ferrous P450; transfer of a second electron to the oxyferrous P450 from NADPH-cytochrome P450 reductase or cytochrome b_5; cleavage of the O-O bond and formation of the highly active species; oxidation of the substrate and followed by the release of the product. Completion of this catalytic cycle involves interactions of P450 not only with the small molecules but also with other electron transfer proteins. Several recent studies further indicated that the above catalytic process might be more complex.[3,4] Hence, at present it is a challenge to fully understand the detailed catalytic mechanism of P450s.

The oxidation reaction catalyzed by P450s occurs in the active site above the heme group. Thus, occurrence of a catalytic reaction requires the substrate first to enter the active site of P450s. After that, the product must leave the active site. During the catalytic cycle of P450s, substrates may also frequently enter and leave the active site.[3,4] To date, crystal structures of more than thirty P450s from different species have been determined, all of which show a similar structural fold at a gross level. Most of the known structures adopt a closed conformation with the active site deeply buried into the cen-

Additional Supporting Information may be found in the online version of this article.

Grant sponsor: Shanghai Natural Science Foundation; Grant number: 10ZR1407000; Grant sponsor: Science Foundation for the Excellent Youth Scholars of East China University of Science and Technology; Grant number: YC0157115); Grant sponsor: Program for New Century Excellent Talents in University; Grant number: NCET-08-0774; Grant sponsor: National S&T Major Project of China; Grant number: 2009ZX09501-001.

Weihua Li and Jie Shen contributed equally to this work.

*Correspondence to: Yun Tang, Department of Pharmaceutical Sciences, School of Pharmacy, East China University of Science and Technology, Shanghai 200237, China. E-mail: ytang234@ecust.edu.cn or Tyuji Hoshino, Graduate School of Pharmaceutical Sciences, Chiba University, Chiba 263-8522, Japan. E-mail: hoshi@p.chiba-u.ac.jp.

Received 3 June 2010; Revised 16 August 2010; Accepted 3 September 2010
Published online 22 September 2010 in Wiley Online Library (wileyonlinelibrary.com).
DOI: 10.1002/prot.22880

ter of the fold. Thus, an intriguing question arises: which part(s) will open up to allow substrate/product passage in the closed form. The question is of importance because substrate recognition and catalytic activity of P450s are influenced not only by the interactions at the P450 active site, but also by the residues far from the active site.[5–11] The issue of substrate access/egress channel in P450s has attracted much attention in recent years.[12–16] Previous molecular dynamics simulations combined with crystal structure analysis suggested a common access/egress channel existing in three bacterial P450s including CYP101, 102A1, and 107A1.[7,17,18] This channel is located between the F-G loop and β1 sheet. The crystal structure of fungal P450 51 exhibits an access channel threading through the B-C loop,[19] which is almost perpendicular to the above channel found in three bacterial P450s. This channel was also identified as the possible channel for an inhibitor egress from the active site of human P450 3A4 by our previous work.[13] In addition, molecular dynamics simulations indicated that other channels might exist in mammalian P450s, most of which are membrane-associated. For instance, a channel located between the helices I and G and the B'-C loop has been suggested to be the possible substrate egress channel in P450 2C5[15] and 2B1.[16] Taken together, these findings have given rise to an idea that different enzymes or classes of P450s may have different routes for substrate entry/egress. Even for a given P450, there might be multiple channels exposed to the exterior solvent or serving as substrate access/egress.

CYP2A6 is one of 57 P450 isoenzymes found in humans, and it can specifically catalyze coumarin 7-hydroxylation.[20] CYP2A6 has been proposed to be a potential drug target for smoking cessation, due to its important roles in the metabolism of nicotine and other tobacco-specific carcinogenic compounds.[21,22] CYP2A6 also showed its potential application in the pharmaceutical industry. Some CYP2A6 mutants have been designed to generate the specific products, which exhibited high inhibitory activity against human protein kinases.[23] The human CYP2A6 is of interest to investigate the substrate channel due to the recently reported experimental results. The kinetic analysis of coumarin catalyzed by CYP2A6 indicated that the oxidation process of the substrate involved rapid substrate binding and release at multiple stages (k_{on} $\sim 10^6 M$/s, k_{off} ~5.7–36/s).[4] This accordingly requires the CYP2A6 structure to open and close rapidly. However, the crystal structure of CYP2A6-coumarin[24] reveals that the substrate is tightly bound in the active site of CYP2A6 and the active site is quite small when compared with other mammalian P450s. No obvious channels are observed for the substrate access/egress. For this reason, the catalytic mechanism of CYP2A6 is not well understood.

In this study, we first probed the potential opening routes in all available crystal structures of CYP2A6. Then we used random acceleration molecular dynamics (RAMD)[15,18] to discover the possible coumarin egress channels in CYP2A6. Based on the channels identified by RAMD, steered molecular dynamics (SMD) simulations[25,26] were then performed to estimate the rupture force and characterize the dynamic process during coumarin egress. To further understand the energetics of coumarin dissociation from the CYP2A6 active site, potentials of mean force (PMF) were also constructed from a number of repeated SMD trajectories using Jarzynski's equality.[27] On the basis of the results from RAMD and SMD, we determined the most likely channel for coumarin egress in CYP2A6. The channel was compared with those identified in other P450s. Finally, the opening mechanism of the most likely channel was described.

MATERIALS AND METHODS

Identification of openings in the CYP2A6 crystal structures

To date, 10 CYP2A6 crystal structures are available in the protein data bank (PDB), including ligand-bound complexes and several ligand-free mutants. The MOLE tool[28] was used to identify the possible openings in the CYP2A6 crystal structures. MOLE uses a Dijsktra path search algorithm to explore the potential channels from a starting point inside the protein to the protein surface. The tool can read a single PDB file or trajectory files generated by MD simulations. The Fe atom in the heme group was set to the starting point for the tunnel search. The number of outcome tunnels was set to five for each structure.

System preparation for MD simulations

The initial structure of CYP2A6 in complex with coumarin for MD simulations was taken from PDB (PDB code 1Z10, at 1.9 Å resolution), which contains four asymmetric 2A6 complex molecules.[24] Molecule A was used for the present MD simulations. The protonation states of charged residues and histidines were determined on the basis of pK_a values calculated by PROPKA.[29] According to the calculation results, His229 and His254 were assigned to be fully protonated at both nitrogen atoms. His72 and His477 were assigned to be protonated at ϵ nitrogen and other histidines to be protonated at δ nitrogen atoms. In addition, Glu448 was set in the protonated state.

The initial structural model of coumarin was extracted from the crystal structure of the CYP2A6-coumarin complex. The model was subjected to geometrical optimization at the B3LYP/6-31G** level using Gaussian03 [www.gaussian.com]. Atomic charges of the substrate were derived using restrained electrostatic potential (RESP) fitting procedure[30] based on the optimized structure. The all-atom model of CYP2A6 complex was generated using the xleap module in Amber8.[31] All crystallization water molecules were kept in the initial model. The resulted model was then solvated with water in a truncated octahedron periodic box. The TIP3P model[32] was used for water, and